In order to determine whether any reasonable mechanism exists for the fluid-dynamic formation of the pit, an attempt was made to measure the boundary-layer thickness at two points in the pit section at station 3. The measurement was carried out by use of the probe, with a hole drilled in the salt beneath it, in order to permit measurements very near the surface.

Figure 4 shows the results of the measurements, together with the results of a similar measurement at a point outside the pit. Apparent velocities different from zero were recorded below the surface of the salt, so that it is obvious that the presence of the hole renders the data meaningless at points very close to the surface. However, it was established in separate tests that the velocity distribution near the outer edge of a boundary layer is measured reliably by use of the technique of Fig. 4. The data were concluded to indicate that the boundary layer within the pit is thinner than that outside.

To be more explicit, the ablation rate at any point on an ablating surface may be expected to depend on the velocity gradient at the surface. This fact follows from the observation that the ablation rate is greater under higher-speed water flows, whereas at the surface itself the water speed is always the same, namely, zero. For making quantitative estimates of the slope, points were carefully located on curves 1 and 2, where the speed was 88% of the largest speeds observed, and the slopes of straight lines from those points to the origin were computed as estimates of the velocity gradients at the surface. The values obtained were 3760 and 3510 ft/in.-sec, respectively. The corresponding figure for curve 3 could not be computed, since the maximum speed was apparently at the salt surface; that is, the estimated velocity gradient would be very large.

If the estimated values of velocity gradient are significant, the ablation rate should be found to be greatest at station 3, rear, and least at station 3, center, with an intermediate rate outside the pit. The order is not at all the same as the magnitudes of the airspeeds outside the respective boundary layers; furthermore, the ratio of the estimated velocity gradients for curves 1 and 2 is 1.07, which is ess than the ratio 1.79 of the maximum air speeds. That is, the boundary layers inside the pit are both thinner than that outside, according to this estimate. The estimated velocity gradients for curves 1 and 2 are, in fact, concluded to be the same, within the limits of uncertainty of the method of estimation employed. Therefore, the ablation rates also are estimated to be equal at the two points and greater for the point of curve 3.

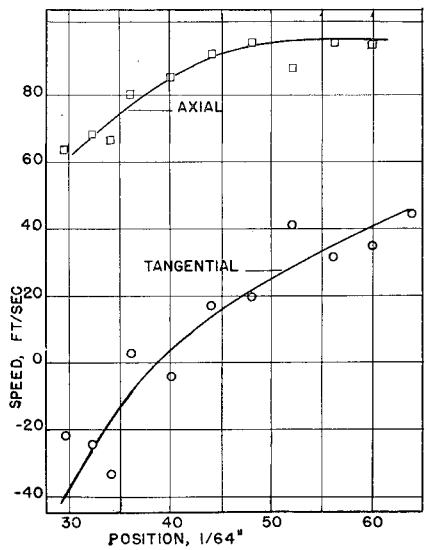

Fig. 3 Axial and tangential components of velocity of flow in the pit at station 4.

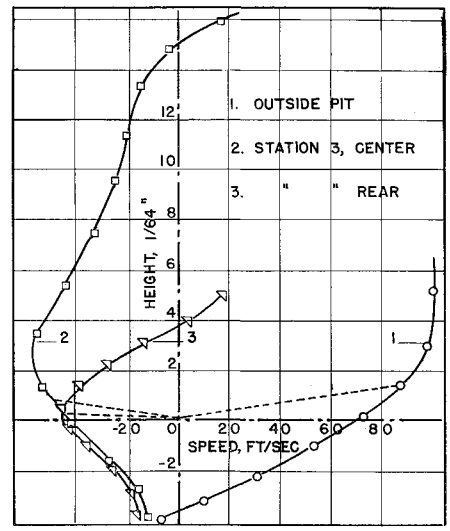

Fig. 4 A comparison of extrapolated velocity profiles (dotted lines) between center and rear edge locations in the pit at station 3, and a point outside the pit immediately upstream of station 3.

It is concluded that 1) measurements of the air flow within a pit, formed by water flow over a salt cake at equal Reynolds number, demonstrate the existence of the vortex flow that has been postulated as causing the formation of the pit; 2) longitudinal flow demonstrated in the vortex is observed to conform to the qualitative predictions of such flow in a stable vortex; 3) the maximum flow speeds inside pits is not high enough to account for pit formation in itself; and 4) measurements intended to determine boundary-layer thickness appear to justify the conclusion that ablation rates in a pit on a salt cake are as high as those outside, because the boundary layer is thinner in the pit as compared to the surface nearby, but outside, the pit.

Reference

[1] Williams, D. T., "A fluid-dynamic mechanism of meteorite pitting," Smithsonian Contrib. Astrophys. **3**, 47–67 (1959).

End Slopes of Column-Beams

JOHN W. HARVEY*
The Bendix Corporation, South Bend, Ind.

Nomenclature

c	=	position ordinate—concentrated load
$j(i)$	=	subscript denoting right (left) end
k	=	index exponent
n	=	series index
w	=	load intensity
x	=	position ordinate
y	=	deflection ordinate
E	=	modulus of elasticity
I	=	moment of inertia
L	=	length
P	=	axial force
W	=	transverse load
α	=	ratio of axial force to critical load $= PL^2/\pi^2EI$
λ	=	algebraic equivalent $= 2L/EI\pi^2$
θ	=	column-beam end slope
τ	=	simple beam end slope
$\phi(\psi)$	=	far (near) end slope magnification factor

Received March 14, 1963; revision received July 23, 1963.

* Engineer, Analytical Services Department, Bendix Products Aerospace Division.

Introduction

EXACT transcendental expressions[1] for the end slopes of simply supported axially loaded prismatic bars subjected to various beam loadings are well known. Application of these functions is facilitated by use of available tables. Related functions for a three moment equation or moment distribution application are computed readily, once the end slope functions are known. This note presents approximate equations for some slope functions derived from series expressions.

All assumptions beyond those of standard column-beam theory are stated as they appear. Compressive forces are taken as positive. The sign convention of the three moment equation is used (see Figs. 1 and 2).

End Couples

A centrally compressed, simply supported bar ij, loaded with a unit end couple, is considered (Fig. 1). The well-known series expression[1] for the elastic curve,

$$y = \lambda \frac{L}{\pi} \sum_{n=1}^{\infty} \frac{1}{n(n^2 - \alpha)} \sin\frac{n\pi x}{L} \tag{1}$$

is not rapidly enough convergent, after differentiation, to insure accuracy with only the first few terms. The convergence is improved[2] by integration below.

The bending moment at an arbitrary section is the sum of the simple beam moment plus the influence of the axial force. Thus,

$$M_x = [(L - x)/L] + Py \tag{2}$$

Integration of the elastic curve equation, where Eq. (1) is substituted into Eq. (2) prior to integration and the series form of the elastic curve for the simple beam curve is used, gives

$$y = \lambda \frac{L}{\pi} \sum_{n=1}^{\infty} \left[\frac{1}{n^3} + \frac{\alpha}{n^3(n^2 - \alpha)}\right] \sin\frac{n\pi x}{L} \tag{3}$$

The procedure is repeated $k - 1$ times, giving the elastic curve:

$$y = \lambda \frac{L}{\pi} \sum_{n=1}^{\infty} \left[\frac{1}{n^3} + \frac{\alpha}{n^5} + \frac{\alpha^2}{n^7} + \ldots \frac{\alpha^k}{n^{2k+1}(n^2 - \alpha)}\right] \sin\frac{n\pi x}{L}$$

By differentiation, the near end slope is

$$\psi \frac{L}{3EI} = \lambda \sum_{n=1}^{\infty} \frac{1}{n^2} + \frac{\alpha}{n^4} + \frac{\alpha^2}{n^6} + \ldots \frac{\alpha^k}{n^{2k}(n^2 - \alpha)} \tag{4}$$

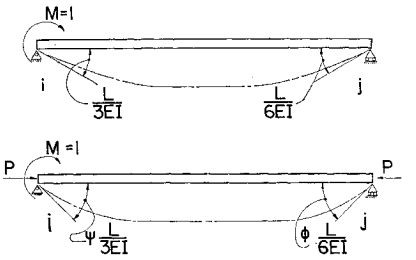

Fig. 1 End slope magnification—applied couple.

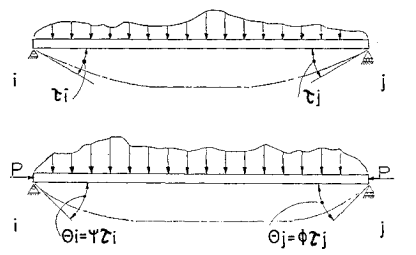

Fig. 2 End slope magnification—general load.

and the far end slope is

$$\phi \frac{L}{6EI} = -\lambda \sum_{n=1}^{\infty} \frac{(-1)^n}{n^2} + (-1)^n \frac{\alpha}{n^4} + (-1)^n \frac{\alpha^2}{n^6} + \ldots (-1)^n \frac{\alpha^k}{n^{2k}(n^2 - \alpha)} \tag{5}$$

Each term, except the last of sequences (4) and (5), is evaluated by Bernoulli's numbers, whereas the last term is approximated by taking $n = 1$. Terminating the sequence after two terms ($k = 1$) gives the near end slope:

$$\psi \frac{L}{3EI} = \lambda \sum_{n=1}^{\infty} \frac{1}{n^2} + \frac{\alpha}{n^2(n^2 - \alpha)} \tag{6}$$

The equivalent

$$\sum_{n=1}^{\infty} \frac{1}{n^2} = \frac{\pi^2}{6} \tag{7}$$

and the approximation

$$\sum_{n=1}^{\infty} \frac{\alpha}{n^2(n^2 - \alpha)} \doteq \frac{\alpha}{1 - \alpha} \tag{8}$$

are introduced into Eq. (6) giving the near end slope magnification factor:

$$\psi \doteq [(1 - 0.392\alpha)/(1 - \alpha)] \tag{9}$$

Similarly, the far end slope magnification factor is

$$\phi \doteq [(1 + 0.216\alpha)/(1 - \alpha)] \tag{10}$$

The accuracy of these expressions is within 2% for compression members with $\alpha < 1$. Less accuracy is realized when the axial force is tensile,† and more than two terms of the sequence may be desirable.

Transverse Loads

Concentrated load

A series expression[1] for the elastic curve of a simply supported column-beam ij, loaded with a concentrated load W, located a distance c from the right support, is

$$y = W\lambda \frac{L^2}{\pi^2} \sum_{n=1}^{\infty} \frac{\sin(n\pi c/L)}{n^2(n^2 - \alpha)} \sin\frac{n\pi x}{L} \tag{11}$$

By the method of the previous section, the end slope at the left end is

$$\theta_i = \tau_i + W\alpha\lambda \frac{L}{\pi} \sum_{n=1}^{\infty} \frac{\sin(n\pi c/L)}{n^3(n^2 - \alpha)} \tag{12}$$

The term τ_i is given by standard formula, whereas the series is approximated by the first term. The sign convention for column-beam end slopes is illustrated in Fig. 2. The near end slope is

$$\theta_i \doteq \tau_i + W\alpha\lambda \frac{L}{\pi} \frac{\sin(\pi c/L)}{1 - \alpha} \tag{13}$$

and the far end slope is

$$\theta_j \doteq \tau_j + W\alpha\lambda \frac{L}{\pi} \frac{\sin(\pi c/L)}{1 - \alpha} \tag{14}$$

Similar functions for various cases of distributed loading are derived by integration of Eqs. (13) and (14). Elimination of the sine term by integration, and the simplicity of the resulting equations dictate the use of magnification factors. In each case the symbol $\psi(\phi)$ denotes the ratio of the column-beam to the simple beam end slope at the left (right) end.

† For tensile loads the sign of α is reversed.

Uniformly distributed load

$$\psi = \phi \doteq [(1 - 0.014\alpha)/(1 - \alpha)] \tag{15}$$

Uniformly varying load

$$\begin{aligned} \psi &\doteq [(1 - 0.076\alpha)/(1 - \alpha)] \qquad \text{load} = w \\ \phi &\doteq [(1 + 0.056\alpha)/(1 - \alpha)] \qquad \text{load} = 0 \end{aligned} \tag{16}$$

The accuracy of these equations is significantly better than Eqs. (9) and (10) because of the integrations involved.

References

[1] Timoshenko, S. P., *Theory of Elastic Stability* (McGraw-Hill Book Co. Inc., New York and London, 1936), 1st ed., Chap. I, pp. 5–30.

[2] Hetényi, M., *Beams on Elastic Foundation* (University of Michigan Press, Ann Arbor, Mich., 1946), 1st ed., Chap. IV, p. 77.

Stress-Intensity Factors for Longitudinal Shear Cracks

G. C. Sih*
Lehigh University, Bethlehem, Pa.

THE concept of crack-tip stress-intensity factors applied to predictions of the fracture strength of cracked cylinders having finite cross sections has been discussed in previous work.[1–3] In this note, the cross sections are assumed to be infinite in extent owing to loads directed along the generators of the cylinder. This problem is of special interest, since it enables the consideration of exact solutions of many configurations, which are inaccessible for cracks under plane extension. Moreover, for cracks under longitudinal shear, it is possible to obtain results that will reveal certain qualitative effects common to all modes of crack surface displacements.

If an infinite body is subjected to longitudinal shear loads, the nonvanishing stress components may be expressed in complex form

$$\tau_{rt} - i\tau_{\theta t} = G(z/\bar{z})^{1/2} f'(z) \tag{1}$$

where r and θ are polar coordinates, t is the coordinate axis directed along the center line of the cylinder, and G is the shear modulus of elasticity. In view of Eq. (1), the state of stress depends only upon the knowledge of a single function $f(z)$ of the complex variable $z = x + iy$.

In order to apply the current fracture mechanics theories to bodies containing crack-like fault lines, it is necessary to obtain the stress distribution near a crack point. For this purpose, an auxiliary complex plane ζ is introduced so that

$$z = \omega(\zeta) \tag{2}$$

maps the crack configuration in the z plane onto the unit circle $|\zeta| = 1$ in the ζ plane. With the aid of Eq. (2), the right-hand side of Eq. (1) is transformed into

$$\tau_{rt} - i\tau_{\theta t} = G\left[\frac{\omega(\zeta)}{\bar{\omega}(\bar{\zeta})}\right]^{1/2} \frac{F'(\zeta)}{\omega'(\zeta)} \tag{3}$$

where

$$f'(z) = \frac{df}{d\zeta}\frac{d\zeta}{dz} = \frac{F'(\zeta)}{\omega'(\zeta)}$$

Received July 22, 1963. Sponsored by the National Science Foundation under Grant NSF-G 24145 with the Lehigh University Institute of Research.

* Associate Professor of Mechanics.

To simplify the analysis, consider the mapping function $\omega(\zeta)$ for a single crack of length $2a$ centered at the origin. It is given by

$$\omega(\zeta) = \frac{a}{2}\left(\zeta + \frac{1}{\zeta}\right) \qquad \zeta = \frac{z + (z^2 - a^2)^{1/2}}{a} \tag{4}$$

The crack tips $z = \pm a$ correspond to $\zeta = \pm 1$ on $|\zeta| = 1$. By way of a translation of the coordinate axes, $z - a = re^{i\theta}$, and restricting attention to a small region around the crack point, where r is small compared to a, Eq. (3) may be written as

$$\tau_{rt} - i\tau_{\theta t} = -[ik_3/(2r)^{1/2}]e^{i\theta/2} + 0(r^{1/2}) \tag{5}$$

in which k_3 is a real parameter. In the course of deriving Eq. (5), $F'(\zeta)$ is assumed to be holomorphic on $|\zeta| = 1$, i.e., the limit of $F'(\zeta)$, as ζ approaches unity, is $F'(1) = -ik_3a^{1/2}/G$. Here, $F'(1)$ is chosen to be purely imaginary so as to satisfy the free surface conditions $\tau_{\theta t} = 0$ for $\theta = \pm\pi$. Now, separating the real and imaginary parts of Eq. (5), the results are

$$\begin{aligned} \tau_{rt} &= [k_3/(2r)^{1/2}] \sin(\theta/2) + 0(r^{1/2}) \\ \tau_{\theta t} &= [k_3/(2r)^{1/2}] \cos(\theta/2) + 0(r^{1/2}) \end{aligned} \tag{6}$$

These equations were obtained earlier by Irwin,[4] who used a different approach. It is of fundamental interest to note that the inverse square-root characteristic of the stress singularity is actually imbedded in the mapping function and is independent of all the other conditions in the problem. Hence, the factor $1/r^{1/2}$ must, of necessity, be common to all crack problems where mapping of the type shown in Eq. (4) is employed. In fact, the conformal mapping technique may be applied to solve a variety of crack problems such as in the cases of plane extension and plate bending.

Now, equating Eqs. (1) and (5) and remembering that Eq. (5) holds only in the limit as z approaches z_1, the crack tip, the stress-intensity factor k_3 may be evaluated from

$$k_3 = i\,2^{1/2}G \lim_{z \to z_1} (z - z_1)^{1/2} f'(z) \tag{7}$$

In the mapped plane, Eq. (7) becomes

$$k_3 = i2^{1/2}G \lim_{\zeta \to \zeta_1} [\omega(\zeta) - \omega(\zeta_1)]^{1/2} \frac{F'(\zeta)}{\omega'(\zeta)} \tag{8}$$

where ζ_1 corresponds to z_1. Thus, a knowledge of $F'(\zeta)$ and $\omega(\zeta)$ in the vicinity of ζ_1 is sufficient to compute k_3.

As an example, consider the problem of an infinite body containing a circular hole of radius b with two collinear cracks of equal depth a originating at the edge of the hole. This configuration can be mapped onto the unit circle in the ζ plane by means of

$$\omega(\zeta) = Z + (Z^2 - b^2)^{1/2} \tag{9}$$

where

$$Z = \frac{R}{2}\left(\zeta + \frac{1}{\zeta}\right) \qquad 2R = a + b + \frac{b^2}{a + b}$$

In this case, the crack tips $z = \pm(a + b)$ on the real axis transform to $\zeta = \pm 1$. At infinity, the body is subjected to longitudinal shear τ^∞, which makes an angle α with the x axis. By virtue of a simple analogy between this problem and the problem in plane hydrodynamics of potential flow,[5] it is possible to construct

$$F(\zeta) = \frac{\tau^\infty R}{G}\left[e^{-i\alpha}\zeta + \frac{e^{i\alpha}}{\zeta}\right] \tag{10}$$

Inserting Eqs. (9) and (10) into Eq. (8) results in

$$k_3 = (a + b)^{-3/2}[(a + b)^4 - b^4]^{1/2}\tau^\infty \sin\alpha \tag{11}$$